

Energy Component Analysis of Electric Field-Induced Shape Change in Water Nanodroplets

Jane Hyojin Lee, Changho Kim,* Mayya Tokman, and Michael E. Colvin

 Cite This: *J. Phys. Chem. C* 2021, 125, 6933–6944

 Read Online

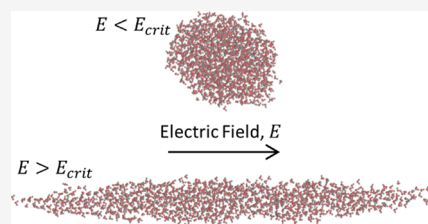
ACCESS |

 Metrics & More

 Article Recommendations

 Supporting Information

ABSTRACT: We present a comprehensive classical molecular dynamics study of water nanodroplets under the influence of an externally applied electric field. Our simulations cover a wide range of droplet sizes and electric field strengths, which allows for a thorough exploration of the structural and energetic behavior of nanodroplets in the presence of an external electric field. Our analysis reveals the molecular-level mechanism behind the shape extension of a nanodroplet from a spheroid to a highly prolate ellipsoid as the propensity of the water dipoles to align with the electric field while simultaneously restructuring to minimize the dipole–dipole interaction energy. We also develop a quantitative theory that describes the energetic landscape for the nanodroplet shape extension process and allows predictions of the nanodroplet behavior based on its initial size and the strength of the applied field.



1. INTRODUCTION

Water's unique combination of small size, near-spherical shape, high polarity, and hydrogen bonding ability enables it to have a large repertoire of possible structures and intermolecular interactions. These properties are key to the myriad functions of water in biochemistry, ranging from stabilizing charged residues and ions to inducing hydrophobic collapse in folding proteins and acting to stabilize reaction intermediates in enzyme active sites. Water's large dipole moment and ability to freely rotate in solution also allow it to interact strongly with external electric fields. At sufficient strengths, external fields can induce electrofreezing in water, which has been observed both experimentally¹ and in computer simulations.² Moreover, previous computational studies revealed that the interaction between water molecules and an external electric field can be the main driver for the initial formation of a transmembrane pore when biological cells are subjected to an electroporation procedure.^{3–7}

The shape deformation and fragmentation behavior of water droplets in strong external electric fields are important aspects relevant to a variety of applications, including electrospinning,⁸ meteorology,⁹ and inkjet printing.¹⁰ While the earliest theoretical research on droplets in electric fields dates back to (at least) Rayleigh's charge instability study¹¹ in the late 19th century, significant advances in understanding were made by Taylor in his work¹² in 1964. He gave a theoretical explanation of the Taylor cone phenomenon where conical tips are formed on liquid drops suspended from capillary tubes and thin jets are emitted from the tips due to external electric fields. He also derived a theoretical model for the response of a liquid drop to the external electric field. By assuming a prolate spheroidal shape and an equilibrium balance between the electric energy and the surface energy, his macroscopic model

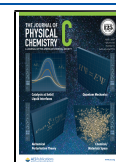
predicts the aspect ratio of the elongated drop at a given electric field strength as well as the critical electric field strength for the onset of the instability. In addition, he predicted that the critical electric field strength is inversely proportional to the square root of the droplet size. Subsequent research showed that introducing a coupling with detailed fluid equations and solving the coupled system numerically yield a more realistic theoretical model for macroscopic droplets.¹³

While experimental and theoretical studies (including those mentioned above) of macro- and microscale water droplets in electric fields have a long history, more recently, advances in technology and science have increased the interest in nanoscale droplets of water. Not only is understanding the general behavior of nanodroplets important in fields such as atmosphere and climate modeling,¹⁴ but more specifically, the dynamics of nanoscale water droplets in electric fields is proving to be of interest for applications as diverse as nanoelectromechanical systems¹⁵ and petroleum dewatering.¹⁶ An interesting question in this context is whether a nanosized droplet of discrete water molecules undergoes shape deformation and exhibits instability in externally applied electric fields as Taylor's macromechanical theory predicts. While extensive molecular dynamics (MD) simulation studies have been conducted to understand the response of nanosized water droplets to an external electric field, those MD studies

Received: January 23, 2021

Revised: March 10, 2021

Published: March 23, 2021



mostly assumed water droplets on a solid surface in the context of electrowetting.^{17–24} As an auxiliary observation to the wettability simulation, the elongation of a free water nanodroplet in an external electric field was reported.¹⁸ However, the electric field used in the MD simulation was not strong enough to investigate the instability behavior predicted by Taylor's theory.

A more relevant MD study was performed for 10 nm-sized free nanodroplets of the small polar organic compound formamide by Luedtke et al.²⁵ It was shown that at a critical strength of an external electric field, there was a sharp structural transition from a nearly spherical shape to a highly extended ellipsoidal structure accompanied by enhanced reorientation of the molecular dipoles in the direction of the electric field. The critical field strengths required for this transition were found to be close to those predicted by Taylor's macroscopic theory. In addition, an electrocrystallization transition was reported for further increased electric fields. It was observed that both transitions exhibit hysteresis when the field is lowered. An analytic-free energy formulation was developed for the variation of the droplet shape as a function of the applied field.

We also note a recent MD study for the deformation of water nanodroplets between two parallel solid plates.²⁴ It was observed that as the strength of an electric field normal to the plates increases, a liquid bridge where the elongated water nanodroplet connects the plates is formed. Conversely, disconnection of the liquid bridge was observed when the electric field was decreased. A hysteresis behavior was observed for this deformation process, which is accompanied by distribution hysteresis of the average dipole orientations of water molecules in the droplet.

In this study, we examine molecular-level structural and energetic details of the water nanodroplet shape transition using an extensive and systematic MD study and a quantitative model analysis. More specifically, the main goals of the paper are as follows. First, we analyze the characteristic behaviors observed in MD simulations of water nanodroplets in electric fields and show that they provide evidence that the shape extension is a field-induced first-order phase transition.²⁶ In addition, we uncover important similarities and differences between the behavior of nanodroplets compared to that of macrodroplets (i.e., droplets with diameter $\geq 1 \mu\text{m}$) exposed to electric fields. Second, based on the examination of the energetics of the nanodroplet simulations, we provide a detailed picture of the energetic landscape of the nanodroplet dynamics and develop a quantitative theory that predicts the behavior of the nanodroplet based on its size and the strength of the external electric field. Our interpretation of shape extension as a field-induced first-order phase-transition phenomenon is reinforced by the emergence of a double-well structure in the potential energy landscape.²⁶

2. MD SIMULATIONS

Using MD simulations, we observe the existence of two different shapes of water nanodroplets that are stable in an external electric field. One is a slightly prolate ellipsoid and the other is a significantly extended ellipsoid with pointy tips. Which shape is stable or whether both shapes are stable depends on the electric field strength as well as the droplet size. To investigate this structural transition behavior, the following two types of MD experiments were performed. In the first, which we call "stretch experiments," a constant electric field is

applied to an initially spherical droplet and the temporal structural changes of the droplet are observed during a fixed simulation time. In the second, which we call "collapse experiments," we start with a highly stretched droplet in a strong electric field, and the field strength is lowered systematically to determine the minimum field that would support the extended form of the droplet. We performed simulations spanning a range of droplet sizes and electric field strengths with multiple replicates for each size/field combination. The MD parameters used for both experiments are described in Section 2.1. The simulation procedures of the stretch and collapse experiments are given in Sections 2.2 and 2.3, respectively.

2.1. Simulation Setup. To observe the structural changes of an isolated nanodroplet in response to an external electric field, we performed all-atom MD simulations using the GROMACS Version 4 program suite.^{27,28} For each simulation, an infinite system containing a single nanodroplet in a vacuum was considered. In other words, instead of imposing periodic boundary conditions, which require approximate treatment of long-range forces, all cutoff distances in the force field were set to infinity and exact long-range forces were used. To avoid floating-point underflow errors resulting from the calculation of Lennard–Jones interactions between widely separated water molecules, the double-precision version of GROMACS was used. We emphasize that our simulation results do not have finite system-size effects that complicate the interpretation of MD simulations. Since the number of water molecules on the surface of a nanodroplet is comparable to the number of water molecules in the "bulk" volume, some aspects of the behavior of a nanodroplet in the electric field would be expected to significantly depend on the size of the simulated system if periodic boundary conditions are employed. We note that some artificial effects of finite cutoff distances were reported for the MD simulation of the shape elongation process of formamide droplets in uniform external fields of varying strengths.²⁵ We also note that analyzing the finite system-size effects requires extensive theoretical and numerical analysis and obtaining practical correction formulas for size effects is not straightforward even for equilibrium MD simulations.²⁹

To thoroughly investigate the behavior of water molecules under the influence of an external electric field, several water models were chosen for our study. The widely used, rigid, nonpolarizable SPC/E water model³⁰ was used in most of the simulations performed for this study. SPC/E is known to yield reasonably good properties such as experimentally confirmed values for density, viscosity, diffusion constant, and dielectric permittivity with a relatively low computational cost. To investigate any significant effects of flexibility and polarizability, MD simulation results of SPC/E (rigid bond lengths and angles) were compared with those obtained from two other water models for the stretch experiment with the smallest droplet (2 nm radius). The flexible SPC/E model (flexible bond lengths and bond angles)³¹ and the SW polarizable water model (rigid bond lengths and angles)³² were selected. The rigid, anisotropic version of the SW water model was chosen because it was reported to yield the best agreement with water properties.³² As described in Section 3.1, no essential differences were observed.

For both the simulations of droplet stretch and droplet collapse, MD initial configurations were prepared using constant-temperature MD simulations (details are given in the sections for each type of experiment). The temperature was

set to 300 K using Bussi et al.'s stochastic temperature coupling algorithm³³ with a time constant of 0.1 ps. For production runs in the presence of the applied electric field, constant-energy MD simulations (i.e., without temperature coupling) were performed. This was appropriate given that the droplets are isolated in a vacuum and the use of infinite cutoffs and 1 fs integration timesteps ensured good energy conservation.

2.2. Stretch Experiment. In the stretch experiment, we studied three different sizes of droplets with radii of 2, 3, and 4 nm. For each size, 10 equilibrium water droplet starting structures were prepared as follows. We first obtained an initial spherical configuration by generating a water box with its sides equal to the diameter of the droplet and removing water molecules outside of a spherical region. We then equilibrated the initial configuration for 1 ns using a constant-temperature MD simulation without an external electric field. After the equilibration process, the MD trajectory was extended for an additional nanosecond, and structures were saved every 100 ps to create 10 different starting structures. The spherical shape and radii of droplets were observed to be maintained after the equilibration process.

During the equilibration process, a small number of water molecules evaporated away from the droplet as would be expected for a droplet in a vacuum. Before starting the production simulations, we removed all evaporated water molecules defined as any monomer, dimer, or trimer of water that was more than 1 nm from any other water molecule in the droplet. After the evaporated water molecules were removed, the initial structures of the 2 nm radius systems (initially 1125 water molecules) had 1119 to 1112 water molecules (loss of up to 1.2% of the original water molecules), the 3 nm radius systems (initially 3789 water molecules) had 3776 to 3766 water molecules (loss of up to 0.6%), and the 4 nm radius systems (initially 8972 water molecules) had 8929 to 8919 water molecules (loss of up to 0.6%). The observed slow loss to evaporation during the 1 ns equilibration shows that this process does not affect the field-induced structural changes occurring at time scales shorter than a few nanoseconds.

Starting from these equilibrated structures, we conducted MD simulations in the presence of a static electric field with strengths ranging from 0 to 1000 MV/m in the direction we denote as +Z. We note that a similar range of electric field strengths has been used in the electrowetting simulation study of a water nanodroplet.²⁴ These simulations were run without temperature coupling. For fields above the critical value for extension, the simulation was run until the droplet shape reached its maximal extended form. For low electric field strengths, where no highly stretched form was observed, simulations were run for at least 1 ns. For electric field strengths close to the critical electric field, the simulation was extended for additional 1 ns to confirm whether shape extension would be observed. For detailed values of simulation parameters of all simulations performed for the stretch experiment, see Table S1 of the Supporting Information.

2.3. Collapse Experiment. The collapse experiment determines the critical electric field strength E_{crit} which is defined as the minimum field strength that would support a highly extended droplet. To create extended droplets in a strong electric field, we first generated spherical droplets with 15 different values of radius r_0 ranging from 1.45 to 4 nm. For each droplet, in order to obtain a highly extended form, we performed a constant-temperature simulation for 500 ps where an external electric field of 1500 MV/m in the +Z direction

was applied. Then, as done for the equilibrium samples of the stretch experiment, evaporated water molecules were removed.

For each of the resulting 15 droplets, E_{crit} was determined using the following two-step procedure. In the first step, a rough value of E_{crit} was determined using a bisection algorithm, that is, for the interval between 200 and 1000 MV/m, it was tested whether the midpoint $E = 600$ MV/m can support the extended droplet. If so, the lower subinterval (between 200 and 600 MV/m) and the midpoint $E = 400$ MV/m were considered for further refinement. Otherwise, the upper subinterval (between 600 and 1000 MV/m) and $E = 800$ MV/m were used. By repeating this procedure, the range where E_{crit} is located was refined. To determine whether the resulting structure still maintains the highly elongated form for a given field strength E , the ratio λ of the vertical to horizontal axis was determined after 250 ps of simulation. For field strengths close to the critical value for which it can take a while for the droplet to settle down to a stable shape, the MD run was extended by another 250 ps. In the second step, for several E values chosen around the roughly determined value of E_{crit} with an increment of 1 MV/m, 1 ns simulations were performed to determine a refined value of E_{crit} . The range of E values used in the second step for each droplet size and the estimated values of E_{crit} are listed in Table S3 of the Supporting Information.

3. RESULTS AND DISCUSSION

In Section 3.1, we present and analyze our MD simulation results. In Section 3.2, we perform an energy component analysis to characterize the competing energy factors in the shape extension process. In Section 3.3, we compare our MD results with Taylor's theory and perform a quantitative analysis by constructing an empirical potential energy model.

3.1. Stretch and Collapse Experiments. Figure 1 illustrates the observed structural changes in two typical trajectories corresponding to weak and strong electric field strengths. In weak fields, the initially spherical droplets become slightly prolate ellipsoids, while if the field strength is high, the spherical droplets extend significantly into elongated ellipsoids

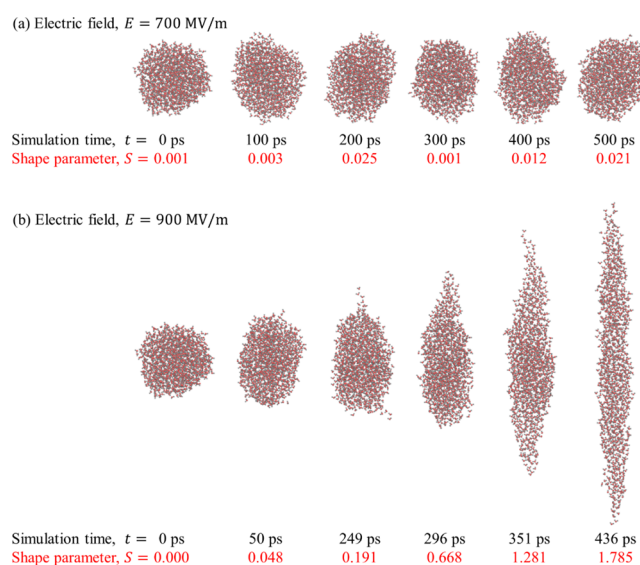


Figure 1. Shape evolution of a droplet with the initial radius $r_0 = 2$ nm for (a) low electric field strength of $E = 700$ MV/m and (b) high electric field strength of $E = 900$ MV/m.

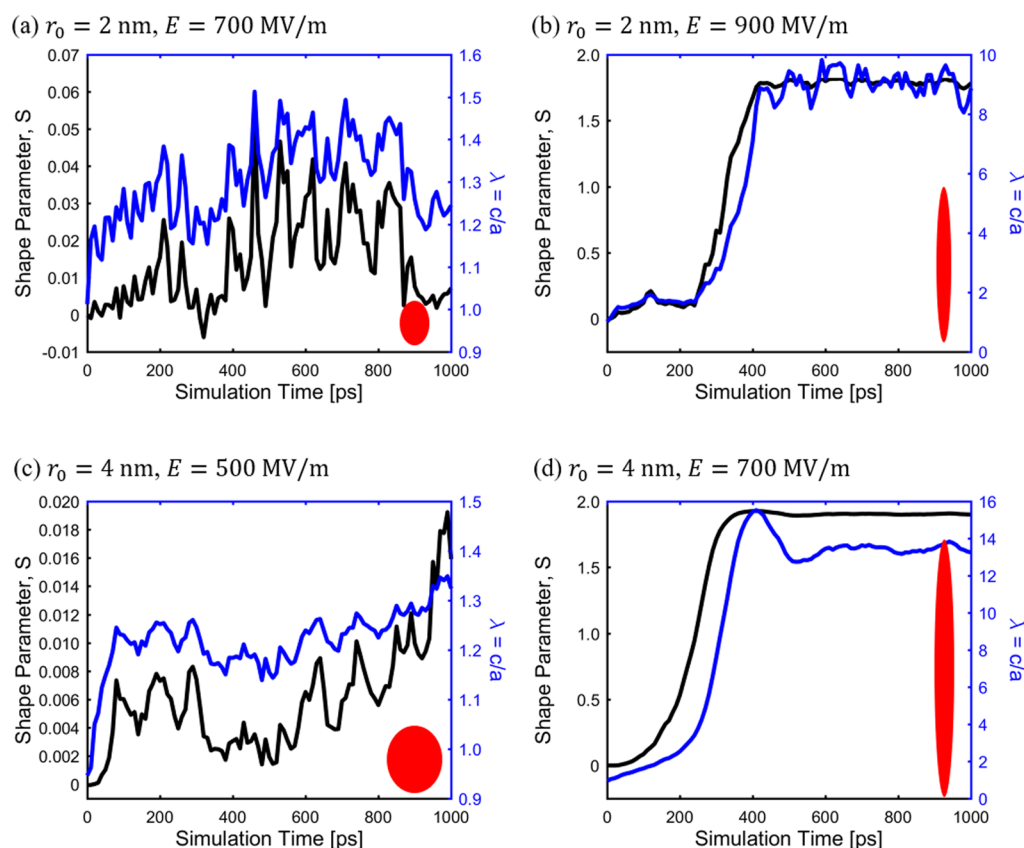


Figure 2. Temporal evolution of the shape parameter S (denoted by black lines) and the ratio λ of major to minor ellipsoid axes (denoted by blue lines) during the stretch experiment. For the initial droplet size $r_0 = 2$ nm, simulation results for electric field strengths (a) $E = 700$ MV/m and (b) 900 MV/m are shown for the shape extension processes leading to slightly prolate and significantly extended ellipsoids, respectively. For $r_0 = 4$ nm, results for (c) $E = 500$ MV/m and (d) 700 MV/m are shown. The red ellipse in each plot shows the vertical cross section of an ellipsoid with a typical value of λ observed in the equilibrated droplet.

with pointy tips. To characterize the shape extension process leading to two disparate shapes, we analyze the temporal evolution of the following two parameters S and λ that are well-defined assuming that the shape of a droplet fits an ellipsoid.

For a given MD configuration formed by a droplet, the shape parameter S^{34} is defined as

$$S = \frac{\prod_{i=1}^3 (\lambda_i - \bar{\lambda})}{\bar{\lambda}^3}$$

where λ_i are the eigenvalues of the gyration tensor and $\bar{\lambda}$ is the average of those eigenvalues. The value of S is bound between $-1/4$ and 2 and it describes in a single value the shape of an ellipsoid. The shape is defined to be an oblate ellipsoid for $-1/4 < S < 0$, a sphere for $S = 0$, and a prolate ellipsoid for $0 < S < 2$. Another parameter $\lambda = c/a$ (note this is not synonymous with the gyration eigenvalues denoted by λ_i and $\bar{\lambda}$ above) is defined as the ratio of the major axis c of an ellipsoid (aligned with the electric field) to the minor axis a (perpendicular to the field direction). The values of principal axes a , b , and c can be determined from the moment of inertia tensor. More detailed information about the calculation of S and λ is provided in Section S2.1 of the Supporting Information.

Figure 2a,b show the temporal evolution of S and λ during the two different shape extension processes for the 2 nm droplet shown in Figure 1a,b, respectively. For the partially extended, slightly prolate ellipsoid case (shown in Figure 2a),

the magnitude of fluctuations in the values of S and λ is relatively large although the average values are different from the sphere to a statistically significant degree. For the highly extended ellipsoid case (Figure 2b), after the rapid increase in the values of S and λ , the shape of the droplet is far from a sphere. Figure 2c,d shows similar results for the case of a larger droplet with a radius of 4 nm.

To systematically investigate the dependence of the field-induced structural change on the initial droplet radius r_0 and the electric field strength E , the temporal evolution of S and λ was analyzed using each set of 10 replicate simulations for the complete ranges of r_0 and E simulated. For the droplets in fields that did not lead to full extension, the time-averaged values are $S \lesssim 0.06$ and $\lambda \lesssim 1.5$, whereas for field strengths where the droplets were elongated, the time-averaged values after the completion of elongation are $S \gtrsim 1.8$ and $\lambda \gtrsim 9$. Detailed time-averaged values of S and λ are listed in Table S2 of the Supporting Information.

The fact that the droplets exist in two distinct structural forms defined by S and λ values in narrow, disjoint ranges suggests that the electrostatic stretching of a nanodroplet may be considered a form of phase transition. In fact, MD simulations indicated that for each value of r_0 , there exists a critical (or threshold) electric field strength E_{crit} such that the droplet becomes only slightly elongated if $E < E_{\text{crit}}$ but highly extended if $E > E_{\text{crit}}$. Simulations performed with $E \approx E_{\text{crit}}$ yielded mixed outcomes, with some simulations leading to extended structures and others not. For example, for $r_0 = 2$ nm,

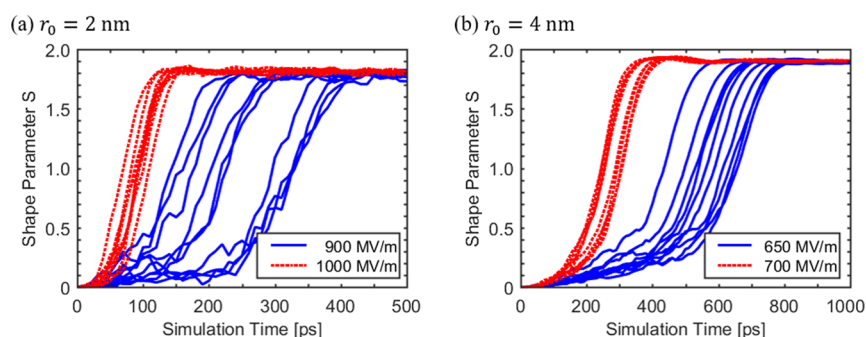


Figure 3. Growth patterns of the shape parameter S observed from 10 replicate MD simulations. To demonstrate the effect of the field strength on the extension dynamics, for each of the initial droplet sizes r_0 , two values of electric field E larger than the critical field E_{crit} are used.

6 out of the 10 replicates provided highly extended ellipsoids and droplets in the rest of the replicates became slightly prolate ellipsoids at $E = 825$ MV/m. This difference in outcomes was observed at $E = 700$ and 622 MV/m, respectively, for $r_0 = 3$ and 4 nm. We first noted that the critical strength decreases as the droplet size r_0 increases. We also observed that the electric field strength exhibiting coexistence of extended and nonextended structures should be given as a range instead of as a single value especially for small r_0 because this range increases as the droplet size r_0 decreases. A more extensive set of simulations validated this observation. For $r_0 = 2$ nm and values of $E = 825, 830, 840, 850, 875,$ and 900 MV/m, we performed 201 replicate simulations for 2 ns. For $E = 825, 830, 840,$ and 850 MV/m, we could observe both fully and slightly extended forms after 2 ns of simulation. On the other hand, for $r_0 = 4$ nm, none of the 10 simulations provided fully extended forms for $E = 619$ MV/m, while all the 10 simulations provided fully extended forms for $E = 625$ MV/m, and the simulations with $E = 622$ MV/m showed coexistence. The coexistence of the two distinct shapes at fields near E_{crit} is a hallmark of phase transitions and the decrease of the coexistence region for a larger system is also consistent with the phase-transition behavior in a finite system.³⁵

One more characteristic behavior of phase transitions is observed from the distribution of extension times. Figure 3 shows the temporal growth patterns of the shape parameter S observed from 10 replicates for two different values of E larger than E_{crit} . While the start time of significant elongation appears to be randomly distributed, the subsequent growth patterns of 10 replicates are similar once significant elongation has started. For E closer to E_{crit} , the distribution of extension times has not only a larger mean but also a larger variance. This is consistent with the typical behavior observed in phase transitions near the critical field strength,^{26,36} where the mean transition/relaxation time is increased (compared to runs at higher fields) and the standard deviation of the distribution is accordingly increased. However, the standard deviation values were observed to be smaller than the mean extension times and not equal as would be expected if the shape extension events exactly follow the Poisson statistics.

We also investigated the alignment of water dipoles in a water droplet equilibrated in the electric field. For each water molecule in the droplet, the angle between the $+Z$ axis and the water dipole was computed and the average was obtained. It is observed that the average angle $\langle\theta\rangle$ decreases as the electric field strength E increases. For $r_0 = 4$ nm, $\langle\theta\rangle$ has a value of $90.01 \pm 0.01^\circ$ at $E = 0$ and it decreases to $52.9 \pm 0.5^\circ$ at $E = 625$ MV/m. Note that $\langle\theta\rangle = 90^\circ$ is expected for $E = 0$ since the

system is isotropic. For $\langle\theta\rangle \approx 53^\circ$ at $E = 625$ MV/m, water dipoles tend to align with a nonzero electric field to stabilize the internal energy of the system. However, the alignment is not perfect due to electrostatic interactions among water molecules. We will investigate these conflicting energy contributions in Section 3.2. The values of the average angle for the whole simulation parameters are listed in Table S2 of the Supporting Information. The surface area of the equilibrated droplet and the water evaporation rate are also listed in that table.

We observed that the two alternate water models we tested, flexible SPC/E and SW polarizable, exhibit essentially the same results (i.e., evident of a phase-transition behavior) (see Table S2 of the Supporting Information). The only major difference was that the shape extension occurs at a slightly different strength of the electric field; for $r_0 = 2$ nm, the coexistence of two shapes was observed at $E = 825$ MV/m for SPC/E and SW, whereas it was observed at $E = 875$ MV/m for flexible SPC/E.

3.1.1. Collapse Experiment. The value of E_{crit} determined by the collapse experiment is observed to decrease as the droplet size increases. While this trend is also observed in the values of E_{crit} measured by the stretch experiment, the latter values are consistently higher than the former values (see Figure 4). In other words, for a given size of a droplet (i.e., containing a certain number of water molecules), a higher electric field strength is required to extend a droplet compared to maintaining an extended droplet. This is consistent with the hysteresis behavior observed in a field-induced first-order phase transition.²⁶ As mentioned in the Introduction, a similar hysteresis behavior was observed for a water nanodroplet

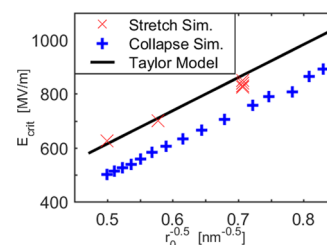


Figure 4. Critical electric field strengths measured/predicted by various methods. Those values are plotted vs $r_0^{-1/2}$. The simulation results from the stretch and collapse experiments are shown by red crosses and blue plus signs, respectively. For the stretch experiment of the droplet size $r_0 = 2$ nm, all electric field strengths that lead to the coexistence of the two droplet forms are plotted as the E_{crit} values. For the Taylor model (black line), eq 2 in Section 3.3.1 is used.

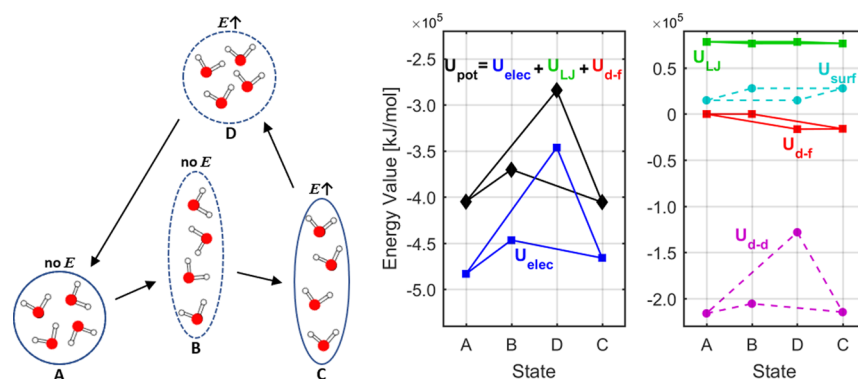


Figure 5. (Left) Energy cycle with four states. (Right) Plots of the values of each energy component in States A, B, C, and D. Note that the physical States A and C are located at the ends of the horizontal axis, whereas the hypothetical States B and D are located between them. The first plot shows the total potential energy (U_{pot}) including all energy terms involved in the MD energy calculations. This plot also shows separately the total electrostatic energy (U_{elec}), illustrating that observed changes in U_{pot} are dominated by the electrostatic term. The rightmost plot separately plots several other components of U_{pot} including the Lennard–Jones (U_{LJ}) and dipole–field ($U_{\text{d-f}}$) energies and the interwater dipole–dipole energy ($U_{\text{d-d}}$), which is one component of U_{elec} . Finally, this plot shows an empirical estimate of the surface tension energy (U_{surf}) described in Section 3.2.

confined between two plates.²⁴ We also note that the relation $E_{\text{crit}} \propto r_0^{-1/2}$ predicted by the Taylor theory holds for E_{crit} values determined by both the stretch and collapse experiments, implying that the equilibrium balance (between the electric energy and the surface energy) used to explain macrodroplets at critical field strengths also holds for nanodroplets.

3.2. Energy Component Analysis. In the previous section, we observed the coexistence of two disparate structures of an isolated water nanodroplet at a critical electric field strength. This observation is a crucial piece of evidence of a structural phase transition and suggests that there are two or more competing factors that stabilize a water droplet in different manners. In this section, we analyze the potential energy terms that drive changes in the overall droplet shape as well as the orientation of the individual water molecules. We analyze the effect of entropy changes on this process separately in Section 3.2.3.

We decompose the total potential energy of the system as $U_{\text{pot}} = U_{\text{LJ}} + U_{\text{elec}} + U_{\text{d-f}}$ where U_{LJ} is the Lennard–Jones interaction energy among water molecules, U_{elec} is the energy of the electrostatic interaction among water molecules, and $U_{\text{d-f}}$ is the interaction energy between the water dipoles and the applied external electric field. In addition, we separately compute the water dipole–dipole interaction energy $U_{\text{d-d}}$, which is part of U_{elec} . Finally, we also compute the surface energy U_{surf} which is defined as the internal energy change to increase the exposed surface area of the droplet. For a given configuration, U_{surf} is computed by multiplying the surface area of the droplet and the surface enthalpy value 123 mJ/m², which is estimated from the surface tension values of SPC/E water at different temperatures.³⁷ The detailed definitions of the energy components are provided in Section S2.2 of the Supporting Information.

In Section 3.2.1, we analyze the changes of the energy components during a hypothetical energy cycle of a water droplet to quantify the main competing energy components involved in the field-induced stretching process. In Section 3.2.2, we investigate the temporal changes in these energy components during the stretch experiment. In Section 3.2.3, we provide some estimates for entropy changes and discuss the free energy changes during the extension process.

3.2.1. Energy Cycle Analysis. The main goal of the energy cycle analysis is to determine the contribution of each energy

component during the shape extension by computing the difference in each energy component between the spherical shape formed at zero electric field and the highly extended shape formed at a strong electric field. Instead of considering only these two physical states, however, we also consider two hypothetical states. This is based on the following observation made in Section 3.1. During the shape extension, not only is the location of the water molecules' centers of mass changed but also the orientation of each water molecule changes to align its dipole moment with the electric field. The former change (in the overall shape) was characterized by increasing the values of S or λ , whereas the latter change (in the distribution of water dipoles) was characterized by decreasing the values of the mean angle $\langle \theta \rangle$ between water dipoles and the + Z axis. To understand the effects of these changes on each energy component separately, we consider the following four states (see the left panel of Figure 5)

- State A: spherical shape with dipoles not aligned ($E = 0$);
- State B: extended shape with dipoles not aligned ($E = 0$);
- State C: extended shape with dipoles aligned ($E > 0$);
- State D: spherical shape with dipoles aligned ($E > 0$).

By computing the potential energy differences during the energy cycle, State A \rightarrow State B \rightarrow State C \rightarrow State D \rightarrow State A, we demonstrate the contribution of each energy component in each state.

For the droplet size $r_0 = 4$ nm (when spherical), we calculated the values of energy components in each state by generating 10 independent configurations. For State A, we obtained these configurations from the 10 equilibrated samples at $E = 0$ MV/m (see Section 2.2). For State C, we obtained those configurations from the 10 stretch experiment simulations at $E = 625$ MV/m, where the configurations of State A were used as initial configurations (see Section 2.2). To obtain the 10 configurations of the hypothetical State B, we fixed the positions of oxygen atoms in the configurations of State C (to keep the extended shape) and performed constrained MD simulations at $E = 0$ MV/m for 100 ps. To relax water dipoles, a simple simulated annealing protocol was employed, where the system temperature was increased to 5000 K during the time interval from 10 to 50 ps. For the

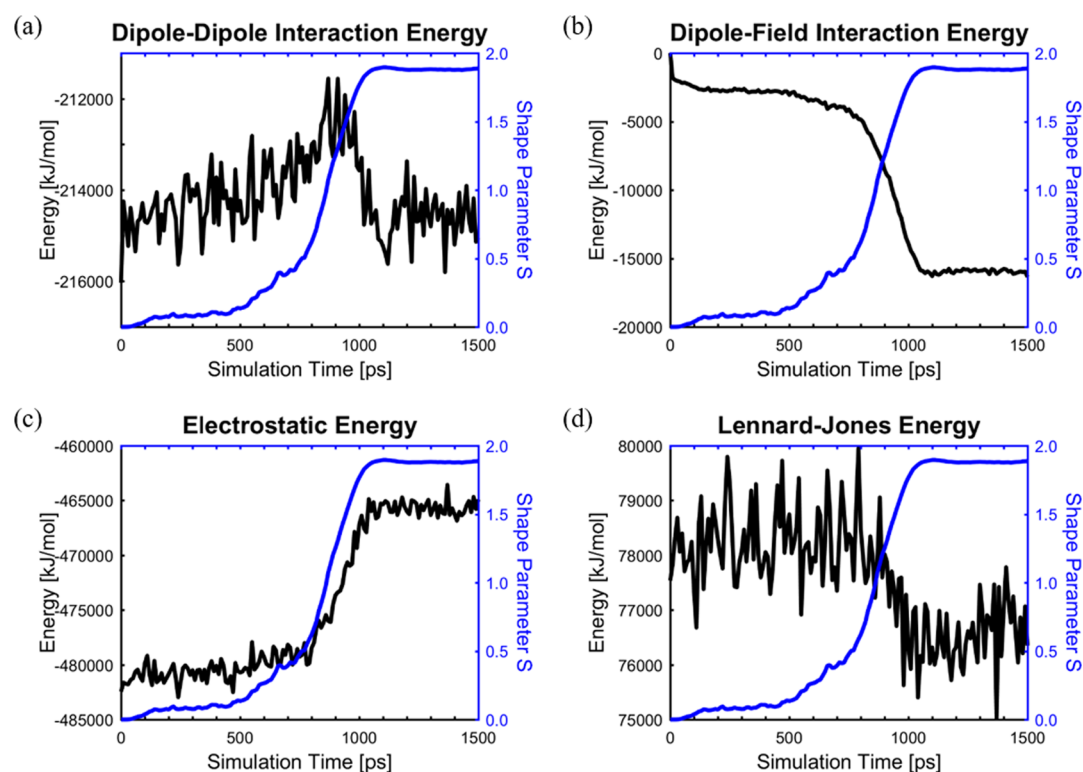


Figure 6. Temporal evolution of the energy components for a sample droplet with the initial radius $r_0 = 4$ nm and the electric field strength $E = 625$ MV/m. All graphs are superimposed on the curve representing the change in the shape parameter S .

hypothetical State D, we performed constrained MD simulations using the configurations of State A and fixing the positions of oxygen atoms for 20 ps. While a very high field of $E = 7500$ MV/m was applied to force alignment of the water dipoles with the electric field so that the mean dipole angle is close to the value observed in State C, the dipole–field energy was computed with $E = 625$ MV/m. The number of water molecules and the mean dipole angle for each state are listed in Table S4 of the Supporting Information.

In the right panel of Figure 5, changes in each energy component during the energy cycle are plotted. The high total potential energy U_{pot} of State D, which is mainly caused by the enormous increase in $U_{\text{d-d}}$, indicates that the spherical shape cannot maintain the alignment of water molecules with the external field due to the unfavorable interaction energy between the adjacent parallel dipoles. However, when the droplet changes shape to an extended ellipsoid, these unfavorable dipole–dipole interactions are largely replaced by favorable stacked parallel dipole–dipole interactions, allowing the water molecules to align with the field. The counterbalancing term is the energetic cost that extends the spherical droplet into an extended ellipsoid, which our analysis shows is partially due to the increased water–vacuum surface area and the reduction in favorable electrostatic interactions within the droplet. The Lennard–Jones (LJ) potential energy, U_{LJ} , is observed not to be as large as the other energy terms. The averaged values of the energy components in each state are listed in Table S4 of the Supporting Information.

3.2.2. Temporal Evolution. The time course of droplet extension and the effect of the field strength on the extension speed are interesting and provide insight into the behavior of this system. Here, we look only at the temporal evolution of the different energy components in a representative droplet

extension (a broader investigation of the kinetics of droplet extension is beyond the scope of this paper, but we are currently completing a study focused solely on that topic). The described energy cycle in Section 3.2.1 clearly shows how the external electric field causes the dipoles to align and the nanodroplet to assume an extended ellipsoidal shape, which is more favorable from the perspective of the dipole–dipole and dipole–field interaction energies. It is also instructive to look at the energetics as the nanodroplet evolves. Figure 6 shows a typical evolution of the energetic components for a nanodroplet of initial radius 4 nm placed in a 625 MV/m electric field (value above $E_{\text{crit}} \approx 622$ MV/m). All graphs are superimposed on the curve representing the change in the shape parameter S to clarify how the shape change is correlated with the changes in the energies.

Figure 6a,b shows that water dipoles align with the electric field and restructure simultaneously to minimize the dipole–dipole interaction energy. While the significant drop in the dipole–field energy $U_{\text{d-f}}$ is the main driver for the deformation into an extended ellipsoid, the change in the dipole–dipole energy $U_{\text{d-d}}$ also contributes to the deformation process as the number of unfavorable parallel dipole–dipole interactions is reduced. However, the overall electrostatic energy U_{elec} , which includes the hydrogen bond interactions, is observed to significantly increase as the droplet is extended (Figure 6c). The LJ interaction energy U_{LJ} does not change significantly although it does exhibit a small decrease (Figure 6d). It is interesting to observe that contrary to other graphs that exhibit either strong correlation or anticorrelation with the time profile of the shape parameter S , the time profile of the dipole–dipole energy $U_{\text{d-d}}$ shows a rather complicated time transient behavior, which may be caused by the strong coupling between dipoles.

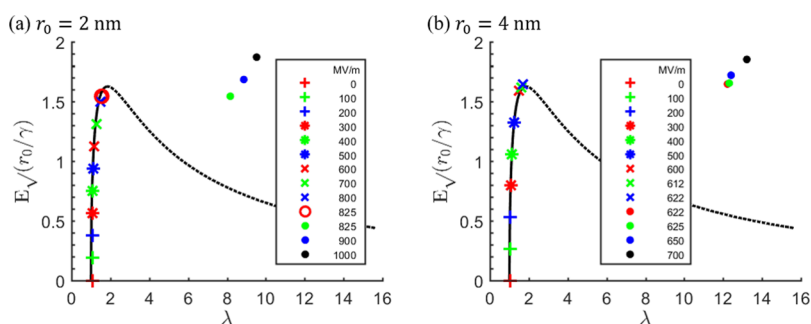


Figure 7. Comparison of the MD simulation results with Taylor's macroscopic theory. The colored symbols denote the MD simulation values of $(\lambda, E\sqrt{r_0/\gamma})$ obtained from the stretch experiment for (a) $r_0 = 2$ nm and (b) $r_0 = 4$ nm. The values in the legends denote the electric field strength E in MV/m. For $E = E_{\text{crit}}$, where both shapes are observed (825 and 622 MV/m for $r_0 = 2$ and 4 nm, respectively), two λ values are plotted; the smaller value is the average among slightly extended droplets, whereas the higher value is that obtained from highly extended droplets. For other E values, we use the averaged values over all 10 replicate simulations. Error bars of the λ values are too narrow to be visible and are thus omitted (see Table S2 in the Supporting Information). The black lines show the curve of $\Phi(\lambda)$ obtained from Taylor's theory, see eq 1. The theory predicts that stable droplets can be found only on the solid lines.

3.2.3. Entropy Contribution. We have so far focused on the changes in energy components of the total potential energy U_{pot} of the system. However, to establish the relative thermodynamic stability of the two shapes of water nanodroplets, we need to compare the free energies of the spherical and extended structures. In contrast to potential energies that can be calculated directly from each static structure in an MD simulation trajectory, the free energies depend on the frequency and conformational degeneracy of the different structures adopted during the simulation and are therefore difficult to calculate. Fortunately, for this relatively simple system, we can estimate the entropy changes associated with the conformational change and dipole orientation. While entropy will eventually drive the system to evaporate, our simulations show that the time scale of evaporation is much slower than that of the shape deformation process so that evaporation can be ignored in our discussion.

For the shape extension process, we consider the following factors for entropy changes. First, due to the surface area change, entropy increases as the droplet elongates. Using the value of surface entropy of 0.20 mN/m·K, which is estimated from the surface tension values of SPC/E water at different temperatures,³⁷ the entropy change is estimated as $T\Delta S_{\text{surf}} = 6.1 \times 10^3$ kJ/mol. The corresponding enthalpy change due to the change in surface area is estimated as $\Delta H_{\text{surf}} = 1.26 \times 10^4$ kJ/mol. The second contribution is due to the alignment of water dipoles. Compared with State A, where water dipoles are randomly distributed ($\langle\theta\rangle = 90^\circ$), State C has lower rotational entropy due to hindered rotations ($\langle\theta\rangle \approx 52^\circ$). Using the model of noninteracting dipoles³⁸ with $\langle\theta\rangle \approx 52^\circ$, we estimated the value of $T\Delta S_{\text{d-f}} = -7.5 \times 10^3$ kJ/mol. The simulation value for the corresponding potential energy change was $\Delta U_{\text{d-f}} = -1.32 \times 10^4$ kJ/mol. The third entropy contribution is from changes in the translational degrees of freedom for the individual water molecules in the spherical and elongated droplets. While this contribution could be estimated from the change in the diffusion coefficient values using the Rosenfeld diffusion-entropy scaling relation or the Adam–Gibbs configurational entropy theory,³⁹ we did not compute them since we did not observe any significant change in water mobility between the different forms.

Hence, the shape extension process involves two main factors that cause entropy changes. The increase in surface area increases entropy and the alignment of water dipoles decreases

entropy. At room temperature (300 K), their overall contributions to the free energy changes are smaller in magnitude than the potential energetic contributions (i.e., the magnitude of enthalpy change is much greater than that of $T\Delta S$). Based on these results, we can assume that the shape extension process can be largely explained by the total potential energy of the system and quantitative energy models based on these terms can be constructed as shown in the next section.

3.3. Quantitative Model Analysis. In this section, using two quantitative models, we analyze the field-induced stretching process of a water nanodroplet observed using MD simulations in Section 3.1. In Section 3.3.1, we first investigate the predictive accuracy of the macroscopic theory of Taylor.¹² In Section 3.3.2, guided by the energy component analysis in Section 3.2, we then construct a potential energy function spanning the conformational change. Using this potential energy function, we explain the observed phase-transition behavior and analyze the critical electric field for droplet extension.

3.3.1. Comparison with a Macroscopic Model. As mentioned in the Introduction, Taylor proposed a macroscopic theory for the stretching of a droplet in an electric field. For specified values of the electric field strength E , the surface tension γ , and the radius of the initial spherical droplet r_0 , the aspect ratio $\lambda = c/a$ of the equilibrium shape is predicted using the relation¹²

$$\begin{aligned}
 E\sqrt{\frac{r_0}{\gamma}} &= \Phi(\lambda) \\
 &= \sqrt{8\pi}\lambda^{-4/3}\sqrt{2 - \lambda^{-1} - \lambda^{-3}} \\
 &\quad \left(\frac{1}{2(1 - \lambda^{-2})^{3/2}} \log \frac{1 + \sqrt{1 - \lambda^{-2}}}{1 - \sqrt{1 - \lambda^{-2}}} - \frac{1}{1 - \lambda^{-2}} \right)
 \end{aligned}
 \tag{1}$$

where electrostatic units are used for $E\sqrt{r_0/\gamma}$. Using eq 1, Taylor also predicted that the critical electric field is given as

$$E_{\text{crit}}^T = \Phi(\lambda_c) \sqrt{\frac{\gamma}{r_0}}
 \tag{2}$$

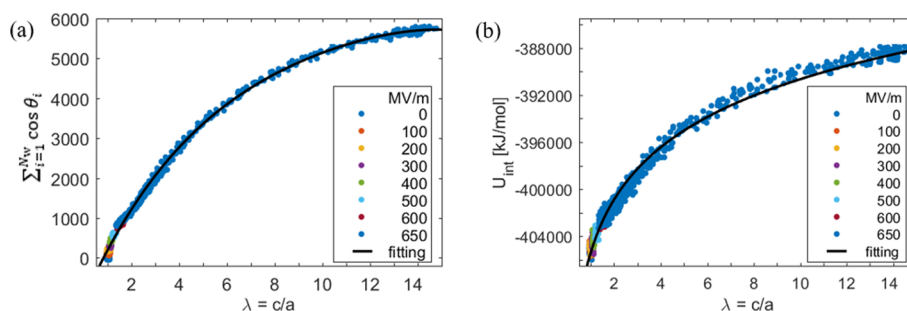


Figure 8. Construction of empirical functions for (a) $\Theta = \sum_{i=1}^{N_w} \cos \theta_i$ and (b) $U_{\text{int}} = U_{\text{LJ}} + U_{\text{elec}}$. Instantaneous values of Θ and U_{int} obtained from the stretch experiment simulations of the droplet size $r_0 = 4$ nm are plotted vs the aspect ratio λ . The values in the legends denote the electric field strength E . Empirical function forms $\Theta(\lambda) = a_4\lambda^4 + a_3\lambda^3 + a_2\lambda^2 + a_1\lambda + a_0$ and $U_{\text{int}} = b\lambda^c$ are used.

where $\lambda_c = 1.86$ is the critical aspect ratio at which $\Phi(\lambda)$ reaches its maximum value. Hence, the theory predicts that $E \leq E_{\text{crit}}^T$ assumes a stable droplet whose aspect ratio λ is given by the relation 1, whereas a droplet becomes unstable at $E > E_{\text{crit}}^T$. In addition, an aspect ratio of $\lambda > \lambda_c$ is not expected to be observed in a stable droplet.

Using the simulation results obtained from the stretch experiment, we investigate the predictive accuracy of relation 1 for nanosized droplets. Figure 7 shows the comparison of the simulation results for $r_0 = 2$ and 4 nm with Taylor's prediction using the surface tension value of SPC/E water³⁷ $\gamma = 63.6$ mJ/m². Until the droplet adopts an equilibrium extended form, the simulation values (λ , $E\sqrt{r_0/\gamma}$) closely match with the curve of $\Phi(\lambda)$. In this case, the values of λ are indeed below $\lambda_c = 1.86$. When E increases beyond the critical value, an abrupt increase in the λ value is observed, and the simulation values (λ , $E\sqrt{r_0/\gamma}$) are located far off from the curve. This behavior is consistent with Taylor's instability analysis. Considering the vastly different droplet size regimes addressed by the two theories, the observed agreement in the results between the MD simulations and the Taylor theory is notable.

However, we note the following differences. First, as shown in Figure 4, while the stretch and collapse experiments give different values of E_{crit} , the Taylor theory, that is, eq 2, predicts only the E_{crit} values obtained from the stretch experiment. Interestingly, the relation $E_{\text{crit}} \propto r_0^{-1/2}$, predicted by the theory, is observed to hold not only for the E_{crit} values obtained from the stretch experiment but also for those from the collapse experiment. Second, contrary to the prediction by Taylor's theory, the nanodroplet reaches an equilibrium state of a highly stretched ellipsoid with pointy tips at high electric fields and the resulting aspect ratio λ is much larger than λ_c . In other words, the Taylor theory cannot explain the coexistence of the two disparate droplet forms nor predict the aspect ratio of a highly extended droplet.

3.3.2. Empirical Potential Energy Model. **3.3.2.1. Construction of $U_{\text{pot}}(\lambda, E)$.** We construct a potential energy function $U_{\text{pot}}(\lambda, E)$ of a water droplet with a specified aspect ratio λ in an electric field E . Based on the observations of the energy component analysis in Section 3.2, we decompose U_{pot} as the sum of the dipole–field energy $U_{\text{d-f}}$ and the internal energy $U_{\text{int}} = U_{\text{LJ}} + U_{\text{elec}}$. For each droplet size $r_0 = 2, 3,$ and 4 nm, we find empirical functions for $U_{\text{d-f}}$ and U_{int} using the simulation results as follows.

When N_w water molecules are placed in an electric field E , the dipole–field energy is expressed as

$$U_{\text{d-f}} = -E\mu \sum_{i=1}^{N_w} \cos \theta_i$$

where μ is the dipole moment of a water molecule, which is constant for a nonpolarizable SPC/E water model, and θ_i is the orientation of the i th water molecule with respect to the electric field direction, where $\theta_i = 0$ means the dipole is perfectly aligned with the field. We assume that $\Theta = \sum_{i=1}^{N_w} \cos \theta_i$ is well approximated by a function of λ . In other words, we express the average orientation of the water dipoles, Θ , in terms of the droplet extension λ , which itself is dependent on the applied field E so that this energy term can be expressed as $U_{\text{d-f}}(\lambda, E) = -\mu E\Theta(\lambda)$.

We further assume that Θ is well described by a polynomial function $\Theta(\lambda) = a_4\lambda^4 + a_3\lambda^3 + a_2\lambda^2 + a_1\lambda + a_0$. To determine the optimal values of the coefficients a_i ($i = 0, \dots, 4$) for each droplet size r_0 by polynomial fitting, instantaneous values of λ and Θ were obtained from the stretch experiment results. From the simulation results with various values of $E < E_{\text{crit}}$, configurations from the final 50 ps were included. Most data points have small values of λ . For larger values of λ , which appear during the shape extension process, simulation results with E slightly larger than E_{crit} were used ($E = 900, 800,$ and 650 MV/m for $r_0 = 2, 3,$ and 4 nm, respectively) and configurations from the initial 100 ps were discarded. Figure 8a shows the simulation results and the fitted curves for $r_0 = 4$ nm.

Applying the same procedure to U_{int} , we determine its empirical functions of the form $U_{\text{int}}(\lambda) = b\lambda^c$ for each droplet size r_0 (see Figure 8b for $r_0 = 4$ nm). Hence, we express the total potential energy as $U_{\text{pot}}(\lambda, E) = U_{\text{d-f}}(\lambda, E) + U_{\text{int}}(\lambda) = -\mu E\Theta(\lambda) + U_{\text{int}}(\lambda)$. The values of the fitting parameters are listed in Table S5 of the Supporting Information. While the chosen empirical forms $\Theta(\lambda)$ and $U_{\text{int}}(\lambda)$ describe the simulation results well for our simulation parameter values, we do not claim that these forms are the only right choices; any smooth function that adequately describes the simulation results would work for our purpose.

3.3.2.2. Double-Well Potential Energy Curve. Using the empirically fitted total potential energy function $U_{\text{pot}}(\lambda, E)$, we analyze the stretching process of a water nanodroplet. We hypothesize that this process is in fact a field-induced first-order phase transition by showing that all relevant observations made in Section 3.1 can be explained based on the field-induced global change of the total potential energy curve.

Both $\Theta(\lambda)$ and $U_{\text{int}}(\lambda)$ increase as the aspect ratio λ increases (see Figure 8), and the dipole–field energy $U_{\text{d-f}} = -$

$\mu\Theta E$ and the internal energy U_{int} are opposing energy terms in U_{pot} as the droplet is stretched. As the electric field strength E increases, energy stabilization via $U_{\text{d-f}}$ becomes dominant leading to a new (meta)stable state with a high aspect ratio value λ . This behavior can be clearly seen from the emergence of a double-well structure in the total potential energy curve versus λ (Figure 9) at certain field strengths. While U_{pot} has a

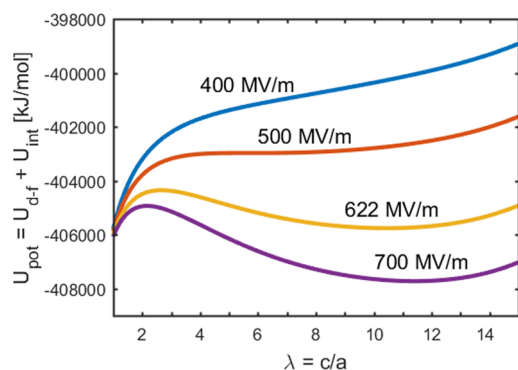


Figure 9. Total potential energy $U_{\text{pot}}(\lambda, E)$. For the droplet size $r_0 = 4$ nm, several curves of $U_{\text{pot}}(\lambda, E)$ are plotted vs the aspect ratio λ for various values of the electric field E . Note that $E = 500$ and 622 MV/m are the E_{crit} values obtained from the collapse and stretch experiments, respectively.

single minimum at $\lambda = 1$ corresponding to small values of E , it eventually acquires another local minimum at $\lambda \gg 1$ as E increases. In addition, the relative stabilities of the two local minimum states depend on E . This explains why the coexistence of the two distinct shapes is observed in the midrange of the electric field values (i.e., near E_{crit}) and only the highly extended shape is observed for larger values of E .

By analyzing the positions and heights of the two local minima in the double-well potential curve of U_{pot} , we make the following observations for each droplet size. First, for each E value greater than the E_{crit} value determined from the stretch experiment, the λ value that shows the second local minimum of the curve is consistent with the average λ value (around 10 to 12) observed from the fully extended droplet in the stretch experiment. Second, at the E_{crit} value determined from the stretch experiment, the two local minima of U_{pot} have similar depths (see Figure 9 for $r_0 = 4$ nm). Lastly, we can use this analysis to predict the electric field at which the second local minimum emerges: 752, 640, and 500 MV/m for $r_0 = 2, 3,$ and 4 nm, respectively. It is interesting to observe that these electric field values are close to the E_{crit} values determined from the collapse experiment although the former values are slightly larger for $r_0 = 2$ and 3 nm.

These observations suggest that the E_{crit} value of the collapse experiment can be predicted as the electric field at which the double-well structure emerges in the potential curve, whereas the E_{crit} value of the stretch experiment can be predicted as the electric field where the stabilities of the two local minima are comparable. Furthermore, the aspect ratio of the fully extended droplet can be predicted from the location of the second minimum in the potential curve.

3.3.2.3. Energetic Barrier Crossing for Droplet Extension. Finally, we investigate the kinetics of the shape extension process. As described in Section 3.1 (see also Figure 3), the average extension time increases monotonically as the electric field is decreased to E_{crit} and there is a considerable variation in

observed extension times among replicate simulations. This behavior can be explained using the stochastic chemical kinetics model³⁶ obeying the simple Arrhenius kinetics. By choosing the aspect ratio λ of the droplet as the reaction coordinate, we can relate shape extension to the random event of energy barrier crossing in the potential energy curve. Then the rate of this random event (which is defined as the reciprocal of the mean extension time) is expressed as

$$\text{rate} = \frac{1}{\langle t_{\text{extend}} \rangle} = ae^{-\Delta U^\ddagger/k_B T} \quad (3)$$

where ΔU^\ddagger is the magnitude of the energy barrier, a is a pre-exponential factor, k_B is Boltzmann's constant, and T is temperature.

Using the constructed total potential energy function U_{pot} , ΔU^\ddagger can be estimated as $U_{\text{pot}}(\lambda^*, E) - U_{\text{pot}}(1, E)$ with λ^* being the barrier location for a given electric field E . Figure 10

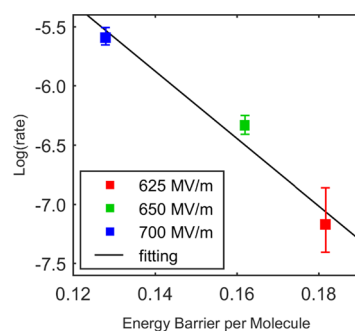


Figure 10. Semi-log plot of the rate of shape extension event (in ps^{-1}) vs the potential energy barrier per molecule (in kJ/mol). Simulation results for the droplet size $r_0 = 4$ nm at three electric field strengths. The linear regression fit is shown as the solid line. Error bars corresponding to two standard deviations for the mean extension time are also plotted.

shows the semi-log plot of the rate versus the energy barrier ΔU^\ddagger for droplet size $r_0 = 4$ nm. As expected from the Arrhenius equation, an approximately linear relationship is observed. This observation underscores that the shape extension process can be interpreted as the random event of energy barrier crossing in the potential energy curve with the double-well structure. We note, however, that the slope of the linear regression was estimated to be $-70/k_B T$ (rather than $-1/k_B T$ as expected from eq 3) in Figure 10, where ΔU^\ddagger was normalized by the number of water molecules. A complexity in describing the reactions involving large groups of molecules is identifying the correct "reaction unit" since the transition from the spherical to the extended form involves the coordinated motion of many interacting water molecules, rather than a single molecular collision. Hence, we estimate the number of water molecules in the "reaction unit" to be approximately 70 water molecules for $r_0 = 4$ nm.

4. CONCLUSIONS

We have presented a detailed study of the structural and energetic behavior of nanodroplets under the influence of an externally applied electric field. A careful analysis of a multitude of simulations revealed the molecular mechanism of the nanodroplet shape extension in the electric field, which can be interpreted as a field-driven first-order phase transition. We found that the transformation of an initially spherical

droplet into a highly extended prolate ellipsoid is due to the tendency of water dipoles to align with the electric field and to reorganize to minimize the dipole–dipole interaction energy. A quantitative theory was developed to predict the shape extension process of a nanodroplet given its initial radius and the strength of the applied electric field. The analysis allowed us to describe the energetic landscape of the nanodroplet transitions between equilibrium states. In fact, it was revealed that at a midrange of critical electric field strengths, two local equilibrium states exist (i.e., slightly and highly extended forms) and the transition between these two states displays an Arrhenius-like behavior. While our MD simulations agree well with the previously known macroscopic mechanical theory in the regime where a droplet is slightly extended, our quantitative analysis also shows significant differences between the behaviors of the nanodroplets versus macrodroplets. It was found that unlike macrodroplets that become unstable at high electric field strengths, the nanodroplets can attain a highly extended form. In summary, based on a combination of empirical and theoretical arguments, we constructed our quantitative model that connects important parameters of the system and predicts the nanodroplet behavior as a function of its initial size and the strength of the external electric field. We believe that the theoretical and computational approach we developed in the current study can be extended to study various phenomena that may be driven by a combination of dipole–dipole and dipole–field interactions including the electrically induced formation of pores in biological membranes^{3–7} and a variety of scientific and engineering applications.^{8–10}

■ ASSOCIATED CONTENT

SI Supporting Information

The Supporting Information is available free of charge at <https://pubs.acs.org/doi/10.1021/acs.jpcc.1c00632>.

List of stretching simulations performed; simulation results of the stretching experiment, the collapse experiment, and the energy cycle analysis; fitting parameter values for the total potential energy function; and descriptions of structural and energetic analyses of a water nanodroplet (PDF)

■ AUTHOR INFORMATION

Corresponding Author

Changho Kim – Department of Applied Mathematics,
University of California, Merced, California 95343, United States; orcid.org/0000-0002-4064-8237;
Email: ckim103@ucmerced.edu

Authors

Jane HyoJin Lee – Department of Mathematics, Stonehill College, Easton, Massachusetts 02357, United States

Mayya Tokman – Department of Applied Mathematics, University of California, Merced, California 95343, United States

Michael E. Colvin – Department of Chemistry and Biochemistry, University of California, Merced, California 95343, United States

Complete contact information is available at <https://pubs.acs.org/doi/10.1021/acs.jpcc.1c00632>

Notes

The authors declare no competing financial interest.

■ ACKNOWLEDGMENTS

The authors gratefully acknowledge computing time on the Extreme Science and Engineering Discovery Environment (XSEDE), which was supported by the National Science Foundation Grant No. ACI-1053575, and the Multi-Environment Computer for Exploration and Discovery (MERCED) cluster at UC Merced, which was funded by the National Science Foundation Grant No. ACI-1429783. J.L. was partially supported by the Stonehill College Conboy Award for Faculty Development program, C.K. and M.T. were partially supported by the UC Merced Academic Senate Faculty Research Grants program, and M.E.C. was partially supported by the Art and Fafa Kamangar Chair in Biological Science at UC Merced.

■ REFERENCES

- (1) Pruppacher, H. R. Electrofreezing of Supercooled Water. *Pure Appl. Geophys.* **1973**, *104*, 623–634.
- (2) Svishchev, I. M.; Kusalik, P. G. Electrofreezing of Liquid Water: A Microscopic Perspective. *J. Am. Chem. Soc.* **1996**, *118*, 649–654.
- (3) Tokman, M.; Lee, J. H.; Levine, Z. A.; Ho, M.-C.; Colvin, M. E.; Vernier, P. T. Electric Field-Driven Water Dipoles: Nanoscale Architecture of Electroporation. *PLoS One* **2013**, *8*, e61111.
- (4) Tieleman, D. P.; Leontiadou, H.; Mark, A. E.; Marrink, S.-J. Simulation of Pore Formation in Lipid Bilayers by Mechanical Stress and Electric Fields. *J. Am. Chem. Soc.* **2003**, *125*, 6382–6383.
- (5) Tieleman, D. P. The Molecular Basis of Electroporation. *BMC Biochem.* **2004**, *5*, 10–12.
- (6) Tarek, M. Membrane Electroporation: A Molecular Dynamics Simulation. *Biophys. J.* **2005**, *88*, 4045–4053.
- (7) Böckmann, R. A.; de Groot, B. L.; Kakorin, S.; Neumann, E.; Grubmüller, H. Kinetics, Statistics and Energetics of Lipid Membrane Electroporation Studied by Molecular Dynamics Simulations. *Biophys. J.* **2008**, *95*, 1837–1850.
- (8) Greiner, A.; Wendorff, J. H. Electrospinning: A Fascinating Method for the Preparation of Ultrathin Fibers. *Angew. Chem., Int. Ed.* **2007**, *46*, 5670–5703.
- (9) Duft, D.; Achtzehn, T.; Müller, R.; Huber, B. A.; Leisner, T. Coulomb Fission: Rayleigh Jets from Levitated Microdroplets. *Nature* **2003**, *421*, 128.
- (10) Kenyon, R. W. Ink Jet Printing. In *Chemistry and Technology of Printing and Imaging Systems*; Gregory, P., Ed.; Springer Netherlands, 1996; 113–138.
- (11) Lord Rayleigh, F. R. S. On the Equilibrium of Liquid Conducting Masses Charged with Electricity. *Philos. Mag.* **1882**, *14*, 184–186.
- (12) Taylor, G. I. Disintegration of Water Drops in an Electric Field. *Proc. R. Soc. Lond. A* **1964**, *280*, 383–397.
- (13) Fontelos, M. A.; Kindelán, U.; Vantzos, O. Evolution of Neutral and Charged Droplets in an Electric Field. *Phys. Fluids* **2008**, *20*, No. 092110.
- (14) Wilhelmsen, Ø.; Trinh, T. T.; Lervik, A.; Badam, V. K.; Kjelstrup, S.; Bedeaux, D. Coherent Description of Transport across the Water Interface: From Nanodroplets to Climate Models. *Phys. Rev. E* **2016**, *93*, No. 032801.
- (15) Wang, F.; Cui, Z.; Li, D.; Ji, B. Bidirectional Regulation of Configuration of the Carbon Nanotube Containing a Water Droplet. *Nanotechnology* **2020**, *31*, 295603.
- (16) Chen, Q.; Ma, J.; Wang, B.; Zhang, Y. Microscopic Mechanism on Coalescence of the Nano-Droplets in Present Non-Uniform Electric Field by Molecular Dynamics Simulations. *AIP Adv.* **2016**, *6*, 115019.
- (17) Yen, T. H. Investigation of the Effects of Perpendicular Electric Field and Surface Morphology on Nanoscale Droplet Using Molecular Dynamics Simulation. *Mol. Simul.* **2012**, *38*, 509–517.

- (18) Song, F. H.; Li, B. Q.; Liu, C. Molecular Dynamics Simulation of Nanosized Water Droplet Spreading in an Electric Field. *Langmuir* **2013**, *29*, 4266–4274.
- (19) Song, F. H.; Li, B. Q.; Liu, C. Molecular Dynamics Simulation of the Electrically Induced Spreading of an Ionically Conducting Water Droplet. *Langmuir* **2014**, *30*, 2394–2400.
- (20) Cao, Q.; Li, L.; Huang, F.; Zuo, C. Ion-Specific Effects on the Elongation Dynamics of a Nanosized Water Droplet in Applied Electric Fields. *Langmuir* **2017**, *33*, 428–437.
- (21) Chan, H. K.; Mak, P. I.; Siu, S. W. I. Exploring the Behaviour of Water Nanodroplet on a Coplanar Electrowetting-On-dielectric: A Molecular Dynamics Approach. *Micro Nano Lett.* **2017**, *12*, 486–489.
- (22) Song, F.; Ma, L.; Fan, J.; Chen, Q.; Lei, G.; Li, B. Q. Electro-Wetting of a Nanoscale Water Droplet on a Polar Solid Surface in Electric Fields. *Phys. Chem. Chem. Phys.* **2018**, *20*, 11987–11993.
- (23) Song, F.; Ma, L.; Fan, J.; Chen, Q.; Zhang, L.; Li, B. Wetting Behaviors of a Nano-Droplet on a Rough Solid Substrate under Perpendicular Electric Field. *Nanomaterials* **2018**, *8*, 340.
- (24) Song, F.; Ju, D.; Fan, J.; Chen, Q.; Yang, Q. Deformation Hysteresis of a Water Nano-Droplet in an Electric Field. *Eur. Phys. J. E: Soft Matter Biol. Phys.* **2019**, *42*, 120.
- (25) Luedtke, W. D.; Gao, J.; Landman, U. Dielectric Nanodroplets: Structure, Stability, Thermodynamics, Shape Transitions and Electro-crystallization in Applied Electric Fields. *J. Phys. Chem. C* **2011**, *115*, 20343–20358.
- (26) Brokate, M. Phase Transitions and Hysteresis. In *Hysteresis and Phase Transitions*; Springer: New York, 1996; 150–174.
- (27) Hess, B.; Kutzner, C.; Van Der Spoel, D.; Lindahl, E. GROMACS 4: Algorithms for Highly Efficient, Load-Balanced, and Scalable Molecular Simulation. *J. Chem. Theory Comput.* **2008**, *4*, 435–447.
- (28) Pronk, S.; Páll, S.; Schulz, R.; Larsson, P.; Bjelkmar, P.; Apostolov, R.; Shirts, M. R.; Smith, J. C.; Kasson, P. M.; Van Der Spoel, D.; Hess, B.; Lindahl, E. GROMACS 4.5: A High-Throughput and Highly Parallel Open Source Molecular Simulation Toolkit. *Bioinformatics* **2013**, *29*, 845–854.
- (29) Kim, K. S.; Kim, C.; Karniadakis, G. E.; Lee, E. K.; Kozak, J. J. Density-Dependent Finite System-Size Effects in Equilibrium Molecular Dynamics Estimation of Shear Viscosity: Hydrodynamic and Configurational Study. *J. Chem. Phys.* **2019**, *151*, 104101.
- (30) Berendsen, H. J. C.; Grigera, J. R.; Straatsma, T. P. The Missing Term in Effective Pair Potentials. *J. Phys. Chem.* **1987**, *91*, 6269–6271.
- (31) Ferguson, D. M. Parameterization and Evaluation of a Flexible Water Model. *J. Comput. Chem.* **1995**, *16*, 501–511.
- (32) van Maaren, P. J.; van der Spoel, D. Molecular Dynamics Simulations of Water with Novel Shell-Model Potentials. *J. Phys. Chem. B* **2001**, *105*, 2618–2626.
- (33) Bussi, G.; Donadio, D.; Parrinello, M. Canonical Sampling through Velocity Rescaling. *J. Chem. Phys.* **2007**, *126*, No. 014101.
- (34) Dima, R. I.; Thirumalai, D. Asymmetry in the Shapes of Folded and Denatured States of Proteins. *J. Phys. Chem. B* **2004**, *108*, 6564–6570.
- (35) Brézin, E. The Onset of Phase Transitions in Finite Systems. *Phys. Bl.* **1986**, *42*, 182–184.
- (36) Hänggi, P.; Talkner, P.; Borkovec, M. Reaction-Rate Theory: Fifty Years after Kramers. *Rev. Mod. Phys.* **1990**, *62*, 251.
- (37) Vega, C.; de Miguel, E. Surface Tension of the Most Popular Models of Water by Using the Test-Area Simulation Method. *J. Chem. Phys.* **2007**, *126*, 154707.
- (38) Langel, W. Orientation Polarization and Hindered Rotation in the View of Thermodynamics. *ChemTexts* **2017**, *3*, 15.
- (39) Dyre, J. C. Perspective: Excess-Entropy Scaling. *J. Chem. Phys.* **2018**, *149*, 210901.